Supporting Information

A KCl-Assisted Pyrolysis Strategy to Fabricate Nitrogen-doped Carbon Nanotube Hollow Polyhedra for Efficient Bifunctional Oxygen Electrocatalysts

Qiannan Liang, Zhijie Chen, Xiaodong Chen, Yingwei Li*

State Key Laboratory of Pulp and Paper Engineering, School of Chemistry and Chemical Engineering, South China University of Technology, Guangzhou 510640, P. R. China.

* Corresponding author. Email: liyw@scut.edu.cn

Contents

Experimental Section

Chemicals. Cobalt nitrate hexahydrate ($Co(NO_3)_2 \cdot 6H_2O$, 99%, Aladdin Industrial Corporation), 2-Methylimidazole ($C_4H_6N_2$, 98%, Aladdin Industrial Corporation), Methanol (CH_4O, 99%, Guangdong Guanghua Sci-Tech Co., Ltd), Ethanol (C_2H_6O, 99%, Guangdong Guanghua Sci-Tech Co., Ltd), Potassium chloride (KCl, Tianjin Damao Chemical reagent Factory), Potassium hydroxide (KOH, 95%, Aladdin Industrial Corporation), Pt/C (20 wt%, Alfa Aesar), IrO_2 (99 wt%, Alfa Aesar) and Nafion (5 wt%, Hesen). All chemicals used in this work were purchased commercially and used without further purification. All the solvents used were of analytical grade.

Synthesis of ZIF-67. Typically, 0.8745 g $Co(NO_3)_2 \cdot H_2O$ and 0.99 g 2-Methylimidazole (2MI) were dissolved in 75 ml methanol, respectively. Subsequently, the 2MI solution was added into the metal salt solution rapidly with vigorous stirring. After stirring for 10 s, the mixture solution was kept still for 24 h at room temperature. The obtained purple precipitates were collected by centrifuging, washed with methanol at least 3 times, and then dried at 60 °C.

Synthesis of NCNHP-r-T. In a typical synthesis, as-prepared ZIF-67 was thoroughly ground with KCl with a mortar (KCl : ZIF-67 = 1:1 by weight). Then the mixture was placed in a tube furnace, heated to 500 °C with a ramp rate of 2 $°C \cdot min^{-1}$ and kept for 3 h under flowing H_2/Ar (1:9) atmosphere. The obtained black powders were washed by deionized water and ethanol and then dried at 60 °C, yielding NCNHP-1-500. A series of samples with different KCl/ZIF-67 mass ratio or carbonization temperature were prepared through a similar synthesis procedure. The products were named as NCNHP-r-T, where r represents the mass ratio of KCl to ZIF-67, T represents the carbonization temperature.

Synthesis of Co/NPC-500. As-prepared ZIF-67 was placed in a tube furnace, heated

to 500°C with a ramp rate of 2 °C·min^{-1} and kept for 3 h under flowing H_2/Ar (1:9) atmosphere. The obtained black powders were washed by deionized water and ethanol and then dried at 60 °C, yielding Co/NPC-500.

Synthesis of Co/NPC-1-500-Ar. The mixture of KCl and ZIF-67 (mass ratio = 1:1) was placed in a tube furnace, heated to 500 °C with a ramp rate of 2 °C·min^{-1} and kept for 3 h under flowing Ar atmosphere. The obtained black powders were washed by deionized water and ethanol and then dried at 60 °C.

Materials characterization. Powder X-ray diffraction (XRD) patterns of the prepared samples were collected with a Rigaku diffractometer (D/MAX/IIIA, 3 kW) employing Cu Kα radiation (40 kV, 30 mA, λ= 0.1543 nm). TGA curves were obtained on TGA550 instrument in nitrogen atmosphere. Raman spectra were recorded on a LabRAM Aramis Raman Spectrometer (HORIBA Jobin Yvon). N_2 adsorption/desorption isotherms were tested at 77 K on a 3H-2000PSI specific surface and pore size analysis instrument. Before the measurements, the samples were degassed in advance. The elemental contents were determined quantitatively by an Elementar Vario EL cube. The surface morphology and size of the materials was investigated by a high-resolution scanning electron microscopy (SEM, SU8220 of HITACHI). The structure and element mapping were determined by a high-resolution transmission electron microscope (TEM, JEOL, JEM-2100F) with EDS analysis (Bruker Xflash 5030T) operated at 200 kV. X-ray photoelectron spectroscopy (XPS) was performed by using Thermo Scientific Escalab 250Xi system with a base pressure of 2 x 10−9 Torr.

Electrochemical measurements. All the electrochemical characterization studies were conducted with a CHI 760E potentiostat (CH Instruments, Inc., Shanghai) supported with the electrochemical station of Pine Instruments (model AFMSRCE) at room temperature. A standard three-electrode system was applied using a glassy carbon rotating disk electrode (GC, RDE) as the working electrode, and a platinum

wire as the counter and Ag/AgCl (3 M KCl) as the reference electrode. The working electrode was prepared with the following procedures. Firstly, 5.0 mg of catalyst was dispersed in 1000 μL of the solution containing 490 μL of ethanol, 490 μL of deionized water and 20 μL of 5wt% Nafion solution and then followed ultrasonication for 30 min to form the homogenous ink. Subsequently, 10 μL of the catalysts ink was uniformly dropped onto the freshly polished glassy carbon electrode (d = 5 mm, S = 0.196 cm^2) with a loading of 0.255 mg cm^{-2}, and dried at room temperature. The measured potentials vs. the Ag/AgCl reference electrode were converted to the reversible hydrogen electrode (RHE) scale via the Nernst equation: $E_{[RHE]} = E_{[Ag/AgCl]} + 0.197 + 0.059$ pH.

OER performance tests. Before evaluating the OER activity, pure O_2 was bubbled through 1 M KOH for 30 min to obtain O_2-saturated solution and catalysts were activated by 60 cyclic voltammetry (CV) cycles at a scan rate of 100 mV s^{-1}. Linear-sweep voltammetry (LSV) measurements were first conducted at a rotating rate of 1600 rpm with a scan rate of 5 mV s^{-1}. Tafel slopes were obtained by plotting overpotential (η) against Log j through LSV curves. The stability of the NCNHP-1-500 was estimated by comparing the LSV curves before and after 1000 CV cycles at a scan of 100 mV s-1 and by chronoamperometric experiments. The electrochemically active surface areas (ECSA) were determined by the double layer capacitance (Cdl) measurements which were performed in non-Faradaic region at different scan rates (4, 8, 12, 16 and 20 mV s^{-1}). Then Cdl was estimated by plotting the Δj at 1.10 V against the scan rate. All the measured OER polarization curve potentials in this work were performed with iR compensation and were converted to reverse hydrogen electrode (RHE).

ORR performance tests. Before the experiments, pure N_2 or O_2 was bubbled through 0.1 M KOH for 30 min to obtain N_2-saturated or O_2-saturated solution, respectively. Cyclic voltammetry (CV) experiments were carried out in N_2- and O_2- saturated solutions with a scan rate of 20 mV s^{-1}. Linear-sweep voltammetry (LSV)

measurements were carried out in the O_2-saturated 0.1 M KOH solution at a rotating rate of 1600 rpm with a scan rate of 10 mV s^{-1}. For rotating ring disk electrode (RRDE) measurements, the disk electrode was scanned catholically at a rate of 5 mV s^{-1}, and the ring electrode potential was held at 1.2 V (versus RHE) to oxidize H_2O_2 diffusing from the disk electrode. The hydrogen peroxide yield [H_2O_2(%)] and the electron transfer number (n) were determined from the following equations.

$$H_2O_2\ (\%) = \frac{200\frac{Ir}{N}}{\frac{Ir}{N} + Id} \quad (1)$$

$$n = \frac{4Id}{\frac{Ir}{N} + Id} \quad (2)$$

where I_d is the disk current, I_r is the current ring current, and N is the current collection efficiency (0.37) of the Pt ring.

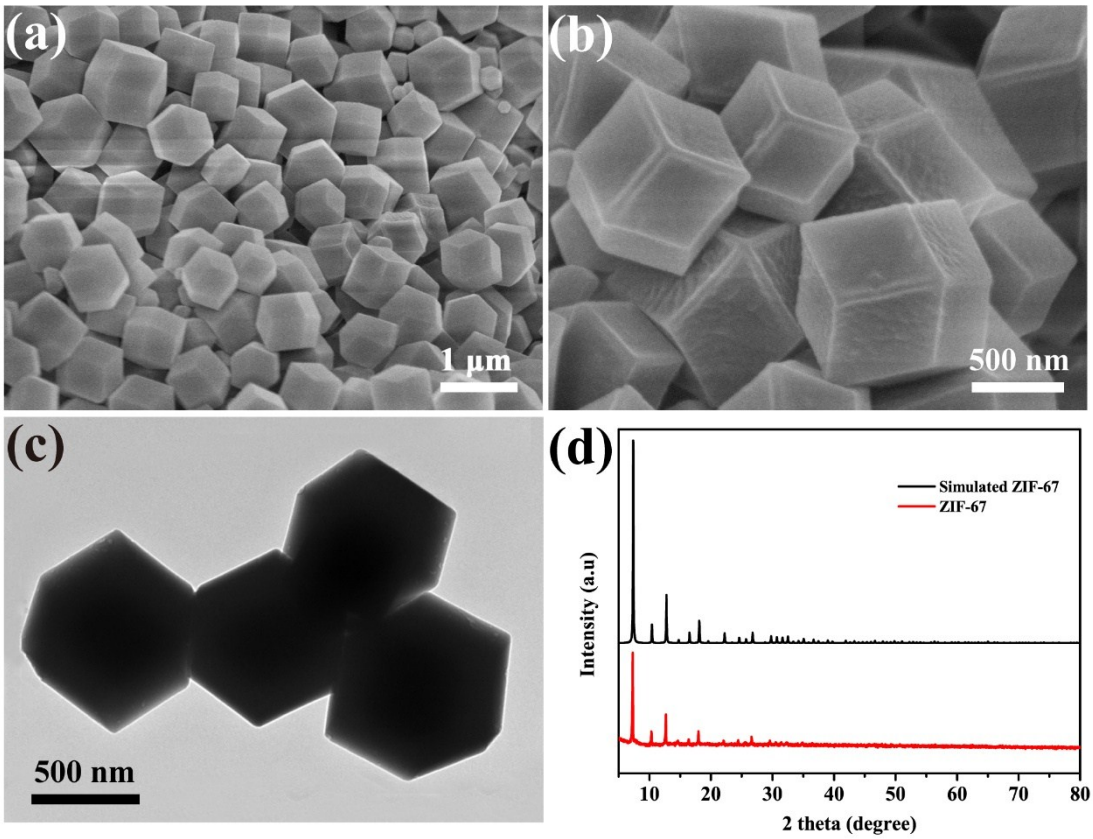

Figure S1. Characterization results of ZIF-67. (a, b) SEM images of ZIF-67, (c) TEM image of ZIF-67, and (d) XRD patterns of experimental and simulated ZIF-67.

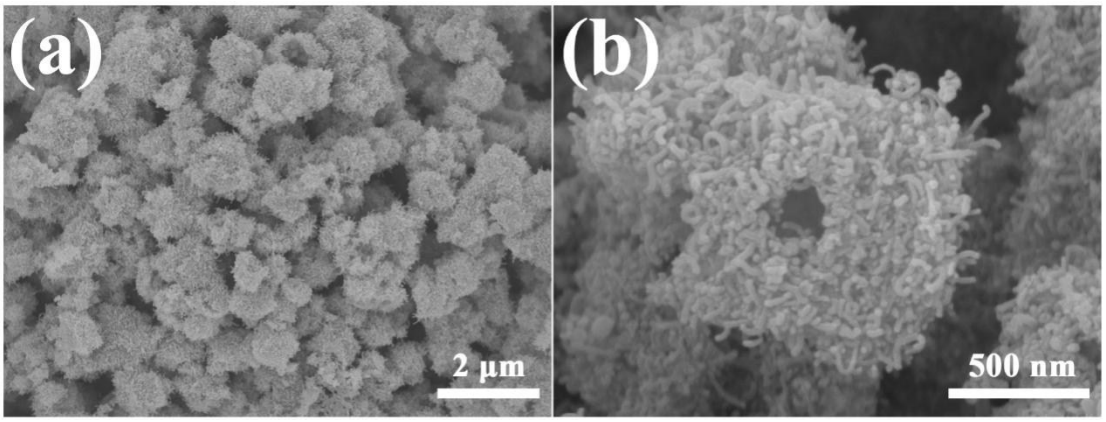

Figure S2. SEM images of NCNHP-1-500.

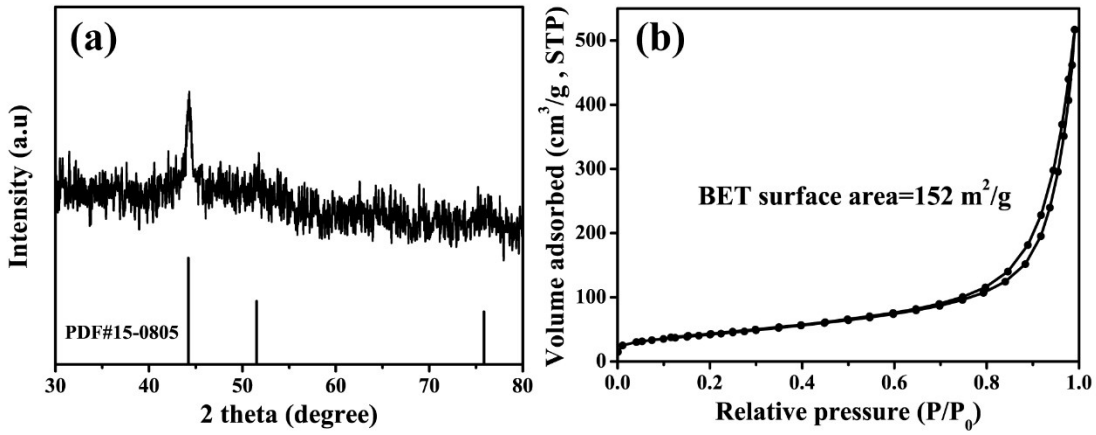

Figure S3. (a) XRD pattern, and (b) N_2 sorption isotherm of NCNHP-1-500.

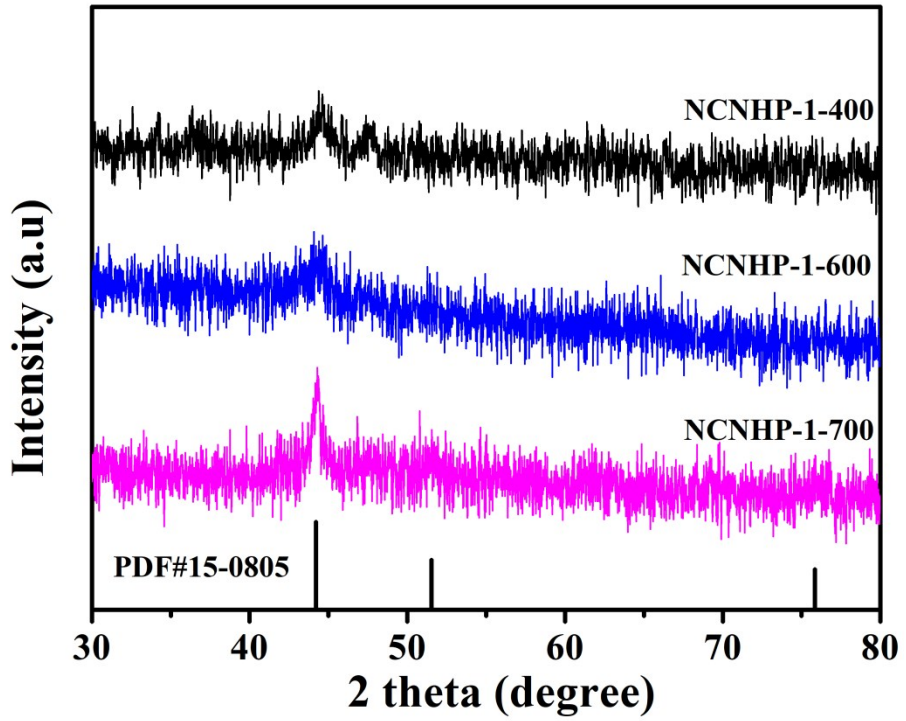

Figure S4. XRD patterns of NCNHP-1-400, NCNHP-1-600 and NCNHP-1-700.

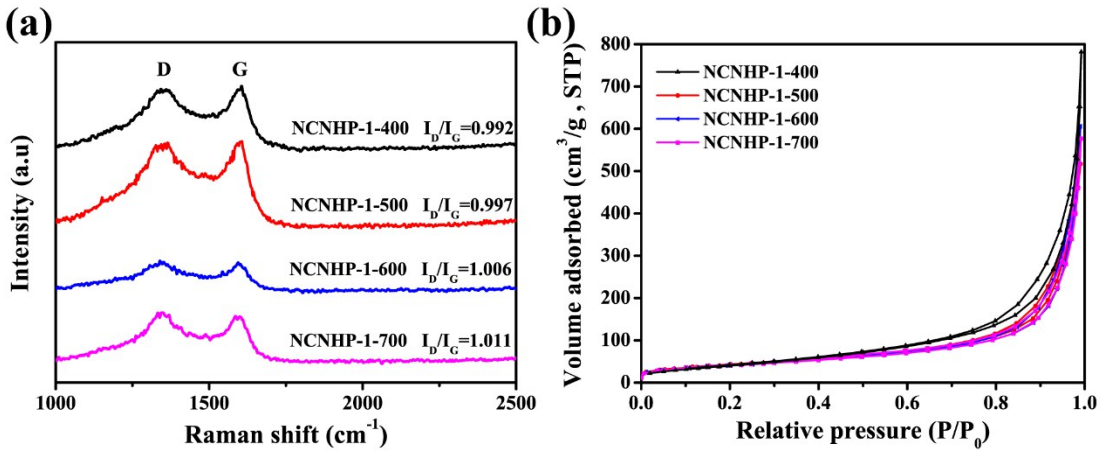

Figure S5. (a) Raman spectra, and (b) N_2 isotherms of the NCNHP samples.

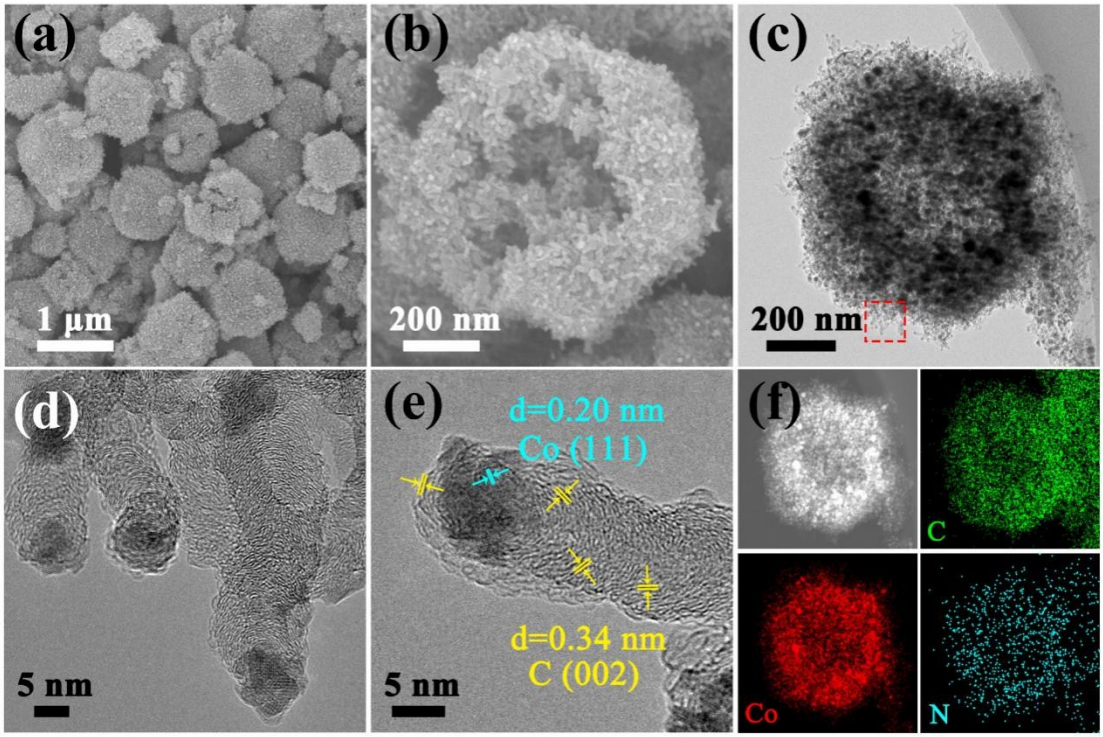

Figure S6. Characterization results of NCNHP-1-400. (a, b) SEM images, (c) TEM images, (d, e) HR-TEM images, and (f) HAADF-STEM and EDS mapping images.

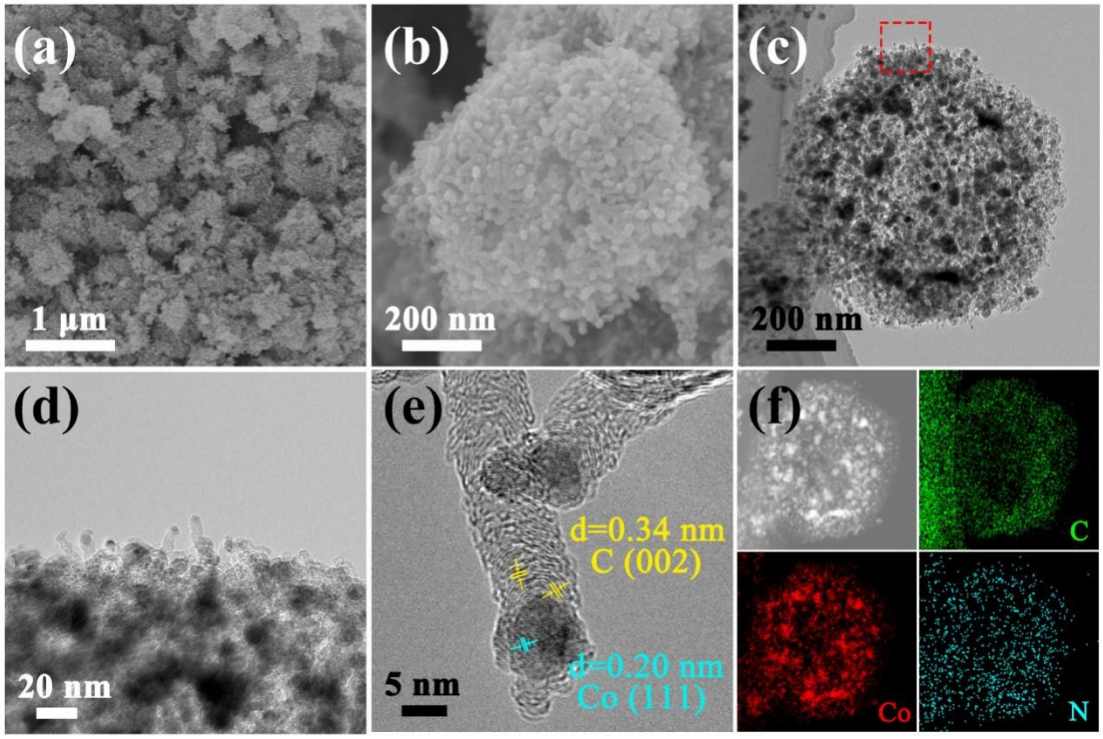

Figure S7. Characterization results of NCNHP-1-600. (a, b) SEM images, (c, d) TEM images, (e) HR-TEM images, and (f) HAADF-STEM and EDS mapping images.

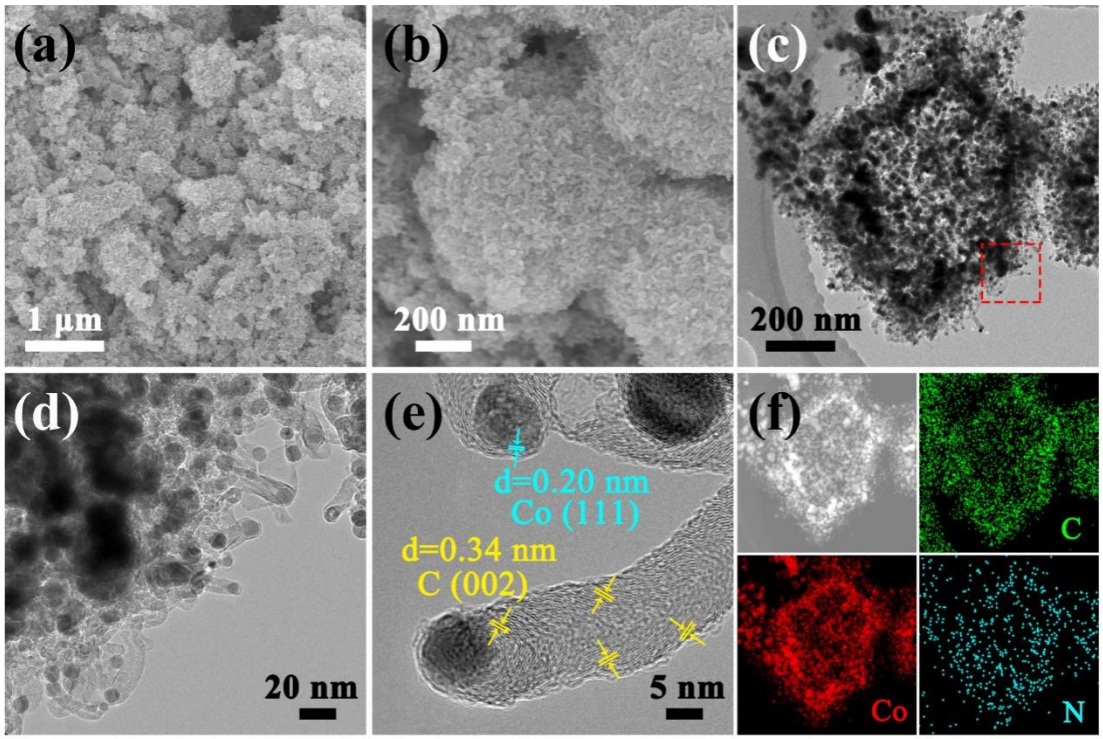

Figure S8. Characterization results of NCNHP-1-700. (a, b) SEM images, (c, d) TEM images, (e) HR-TEM images, and (f) HAADF-STEM and EDS mapping images.

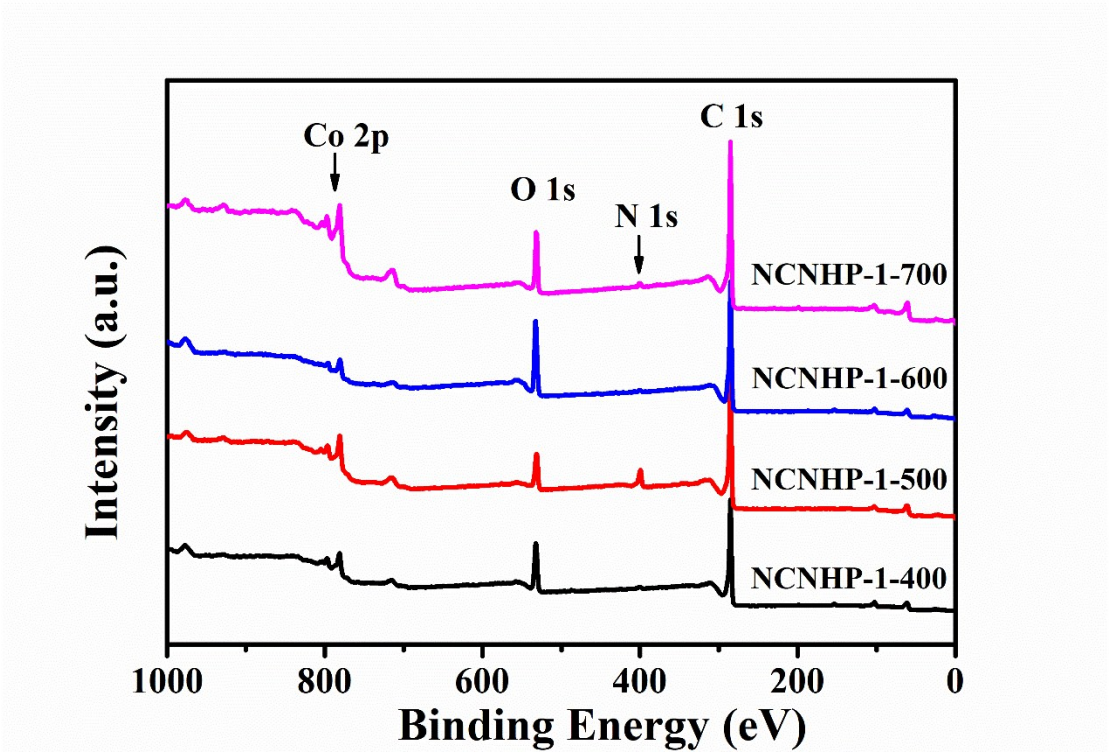

Figure S9. XPS full scans of NCNHP-1-400, NCNHP-1-500, NCNHP-1-600 and NCNHP-1-700.

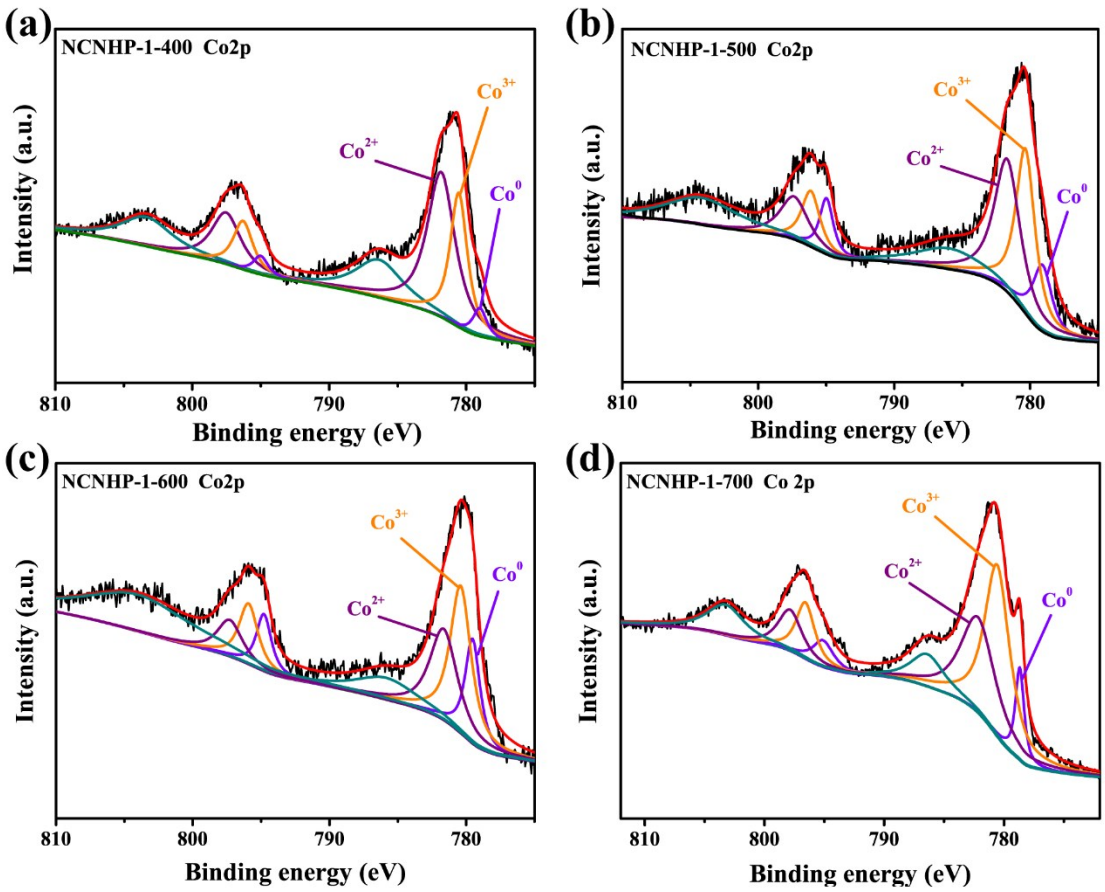

Figure S10. High-resolution XPS spectra of Co 2p of the NCNHP materials.

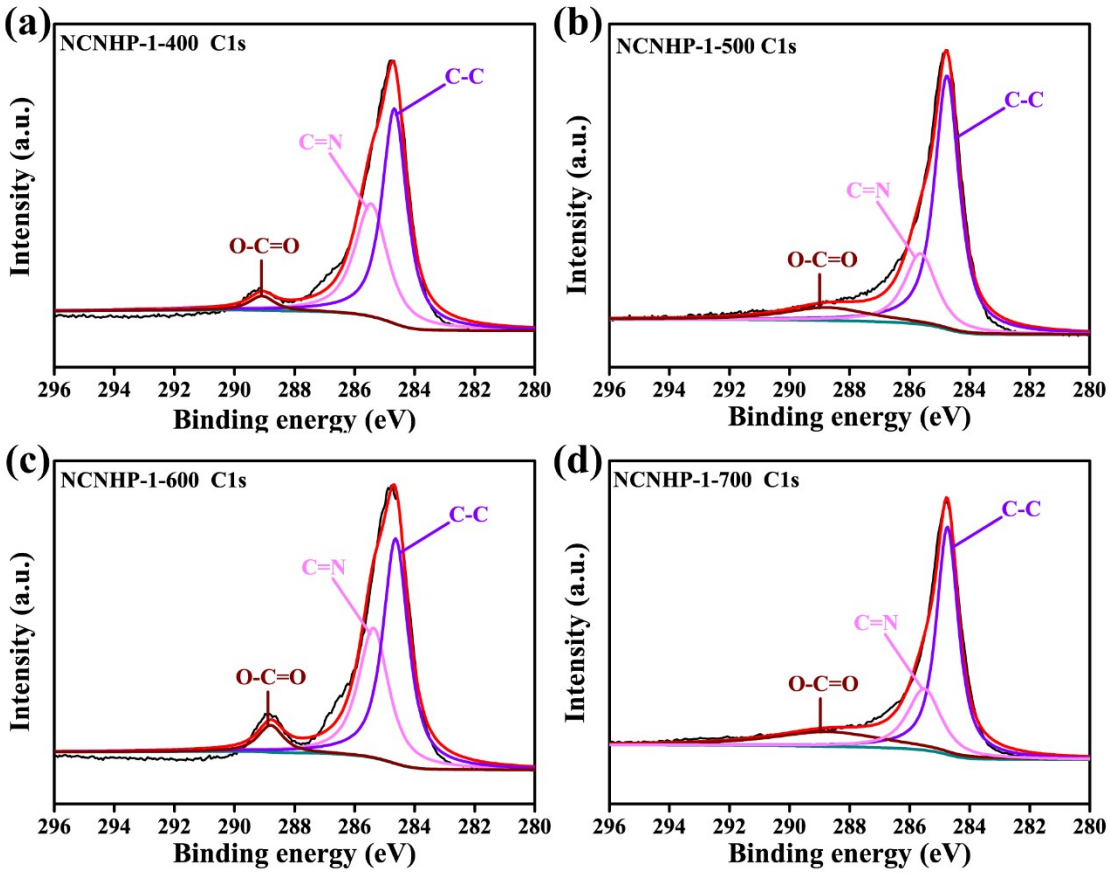

Figure S11. High-resolution XPS spectra of C 1s of the NCNHP materials.

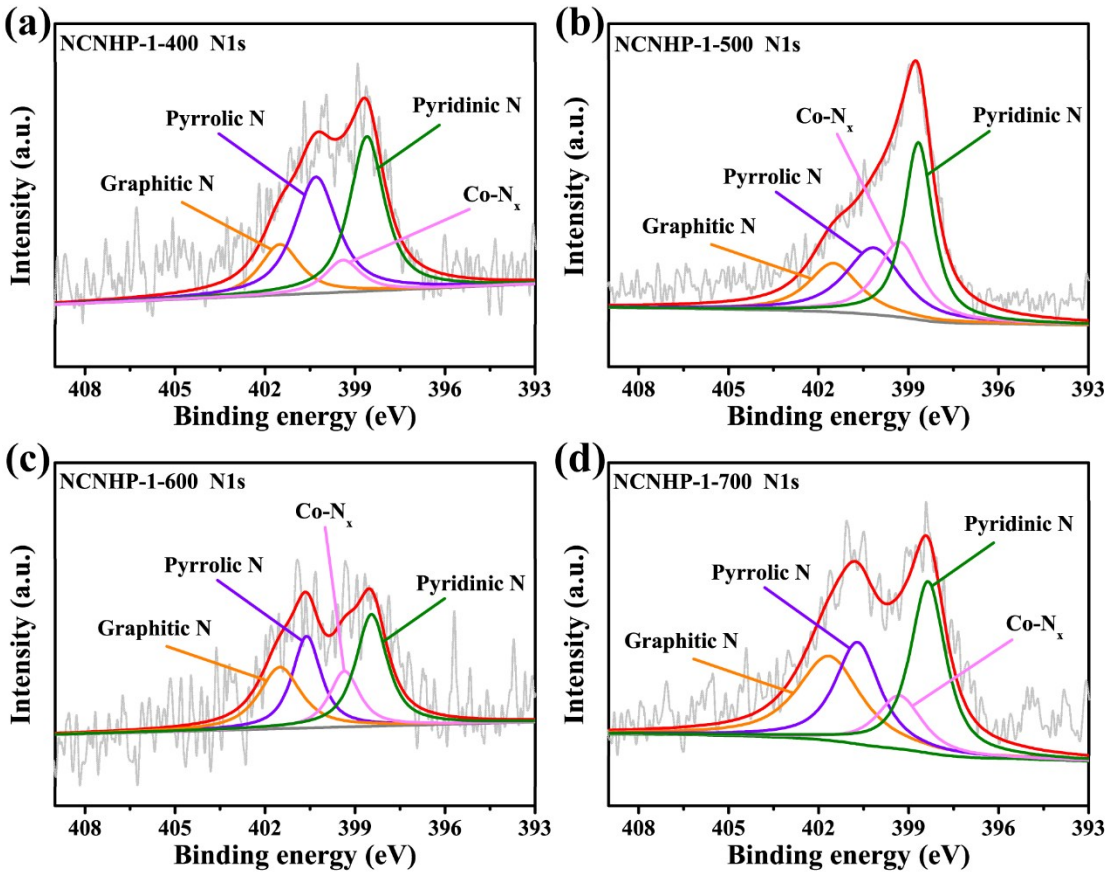

Figure S12. High-resolution XPS spectra of N 1s of the NCNHP materials.

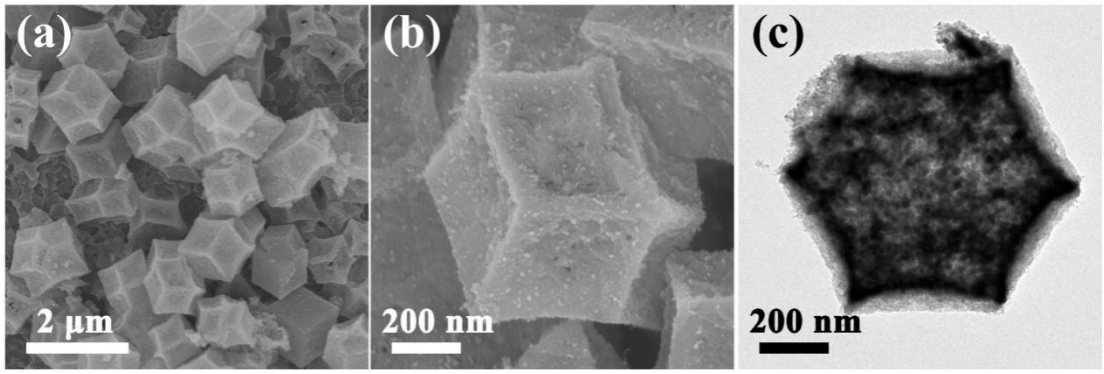

Figure S13. (a, b) SEM images of Co/NPC-500, and (c) TEM image of Co/NPC-500.

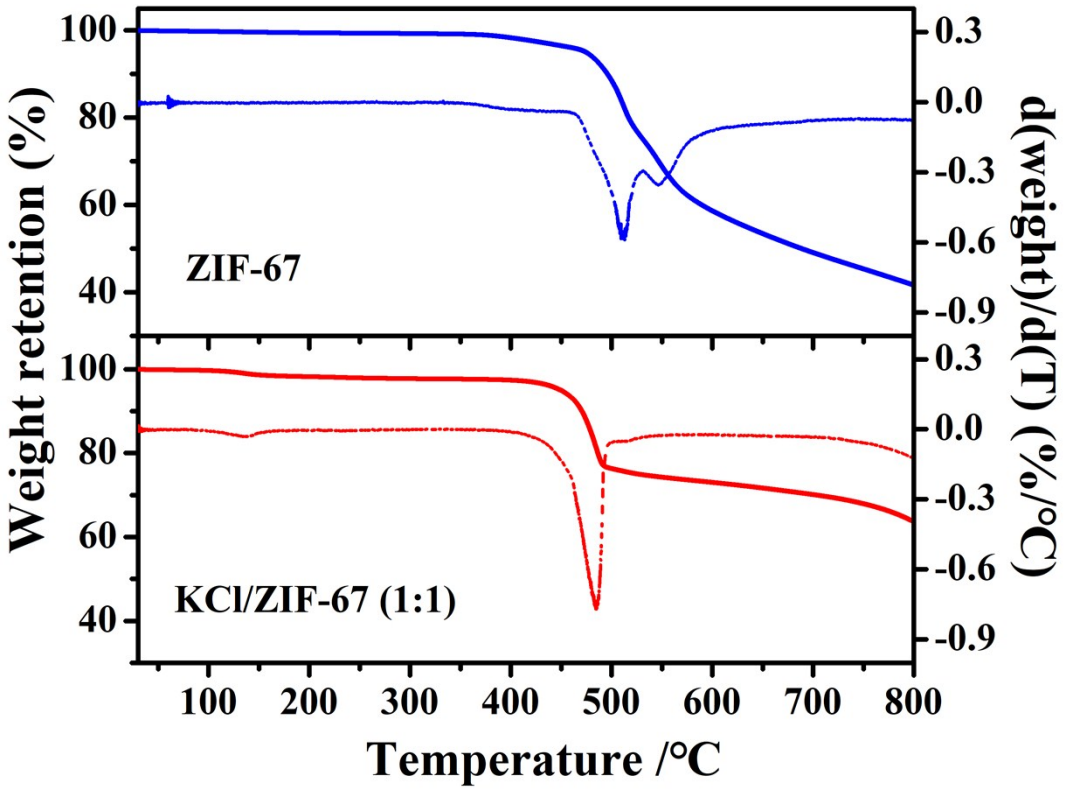

Figure S14. TGA and DTG curves of ZIF-67 and KCl/ZIF-67 mixture (1:1) in N_2 atmosphere.

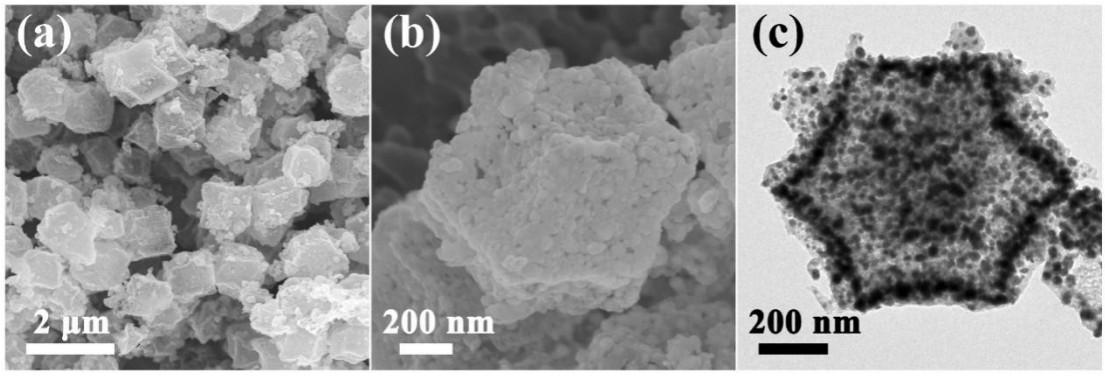

Figure S15. (a, b) SEM images of Co/NPC-1-500-Ar, and (c) TEM image of Co/NPC-1-500-Ar.

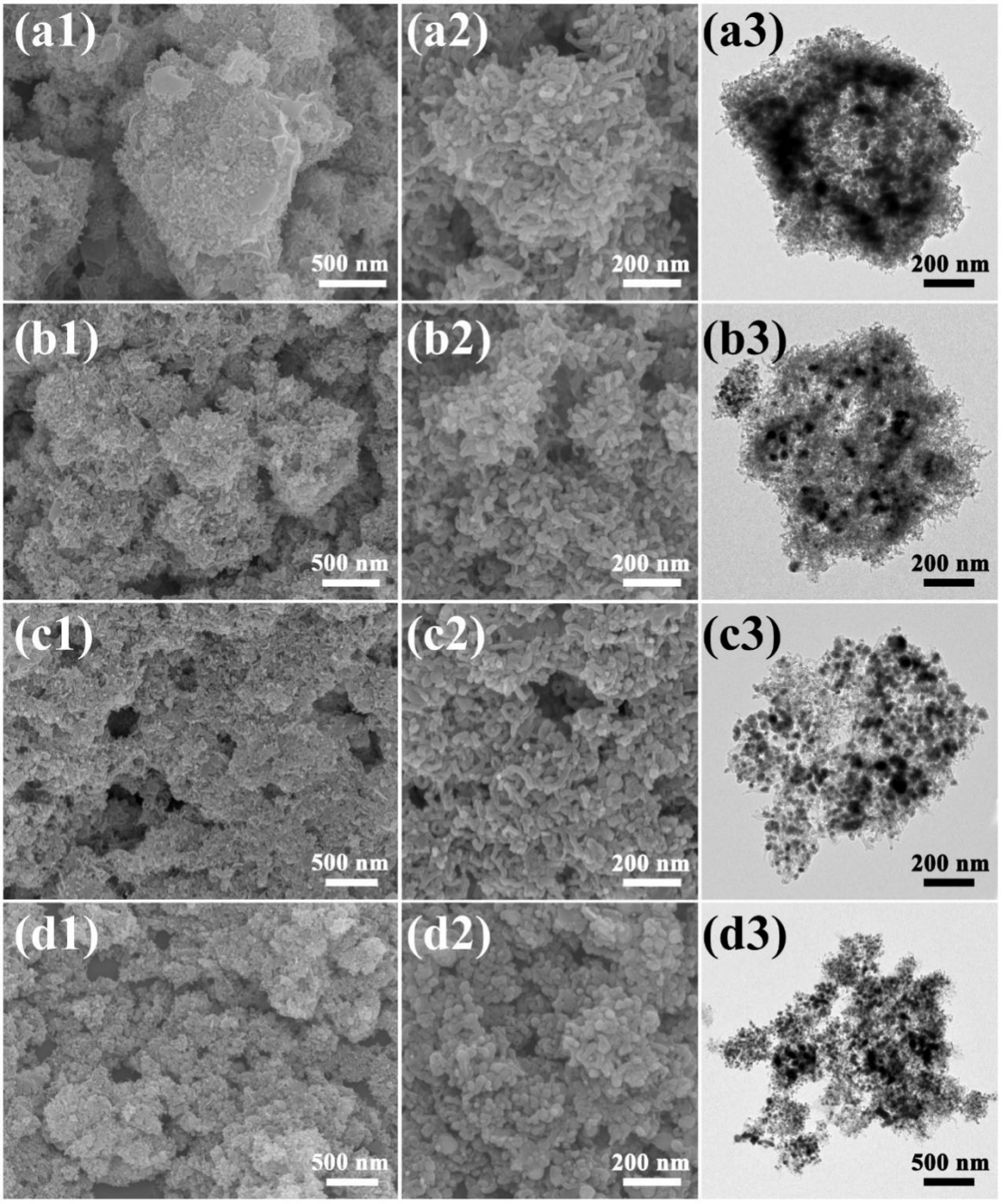

Figure S16. SEM images of (a1, a2) NCNHP-0.5-500, (b1, b2) NCNHP-2-500, (c1, c2) NCNHP-5-500, and (d1, d2) NCNHP-10-500; TEM images of (a3) NCNHP-0.5-500, (b3) NCNHP-2-500, (c3) NCNHP-5-500, and (d3) NCNHP-10-500.

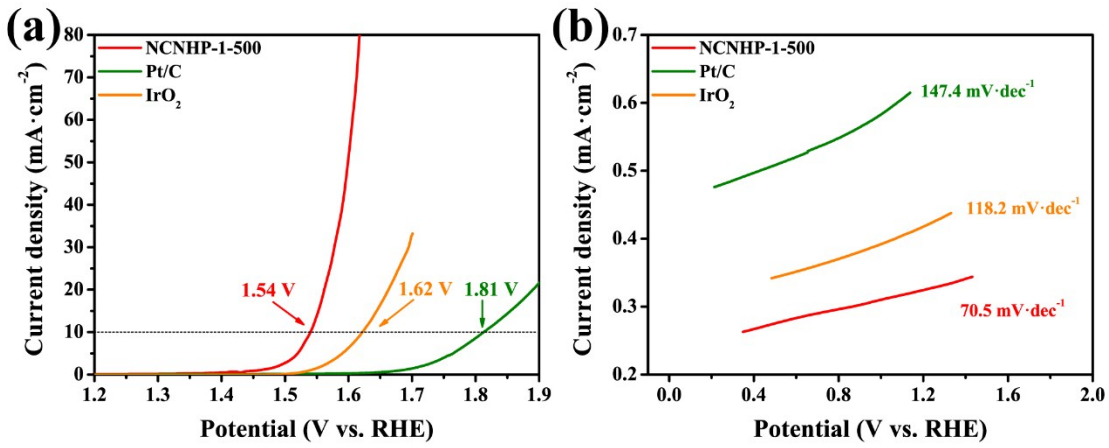

Figure S17. (a) LSV curves and (b) Tafel curves of NCNHP-1-500, Pt/C and IrO_2 in 1 M KOH for OER.

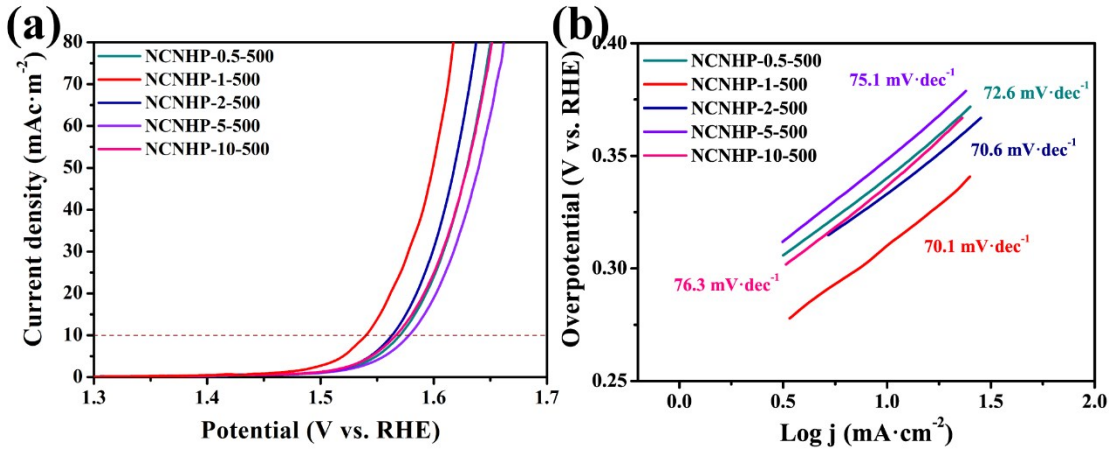

Figure S18. (a) LSV curves and (b) Tafel curves of catalysts prepared by using different ZIF-67/KCl ratio in 1 M KOH for OER.

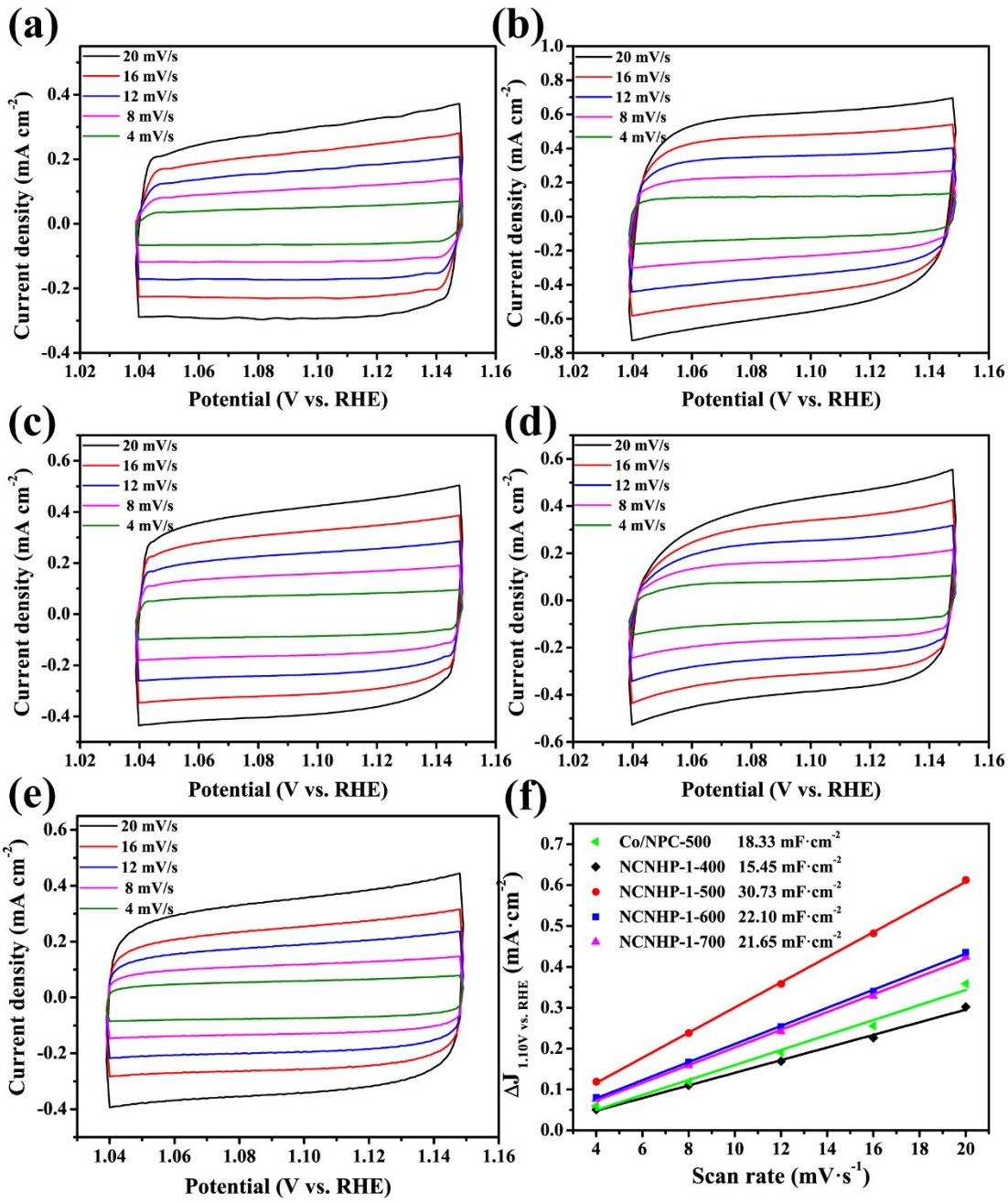

Figure S19. CV curves of (a) NCNHP-1-400, (b) NCNHP-1-500, (c) NCNHP-1-600, (d) NCNHP-1-700, (e) Co/NPC-500 at various scan rates; and (f) electrochemical active surface areas.

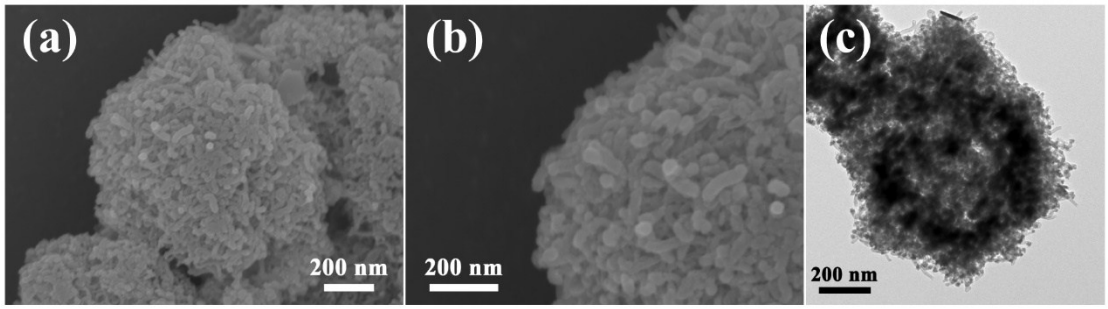

Figure S20. (a, b) SEM images and (c) TEM image of NCNHP-1-500 after stability test for OER.

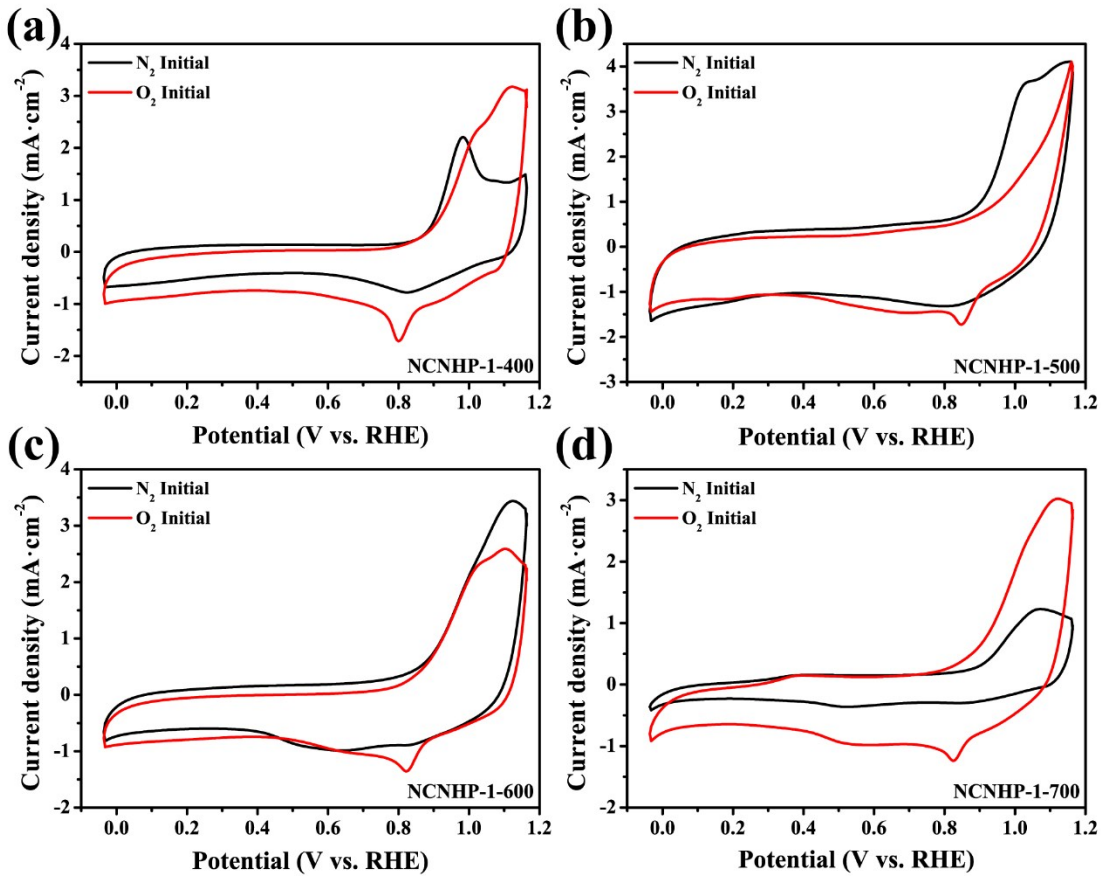

Figure S21. CV curves of (a) NCNHP-1-400, (b) NCNHP-1-500, (c) NCNHP-1-600 and (d) NCNHP-1-700.

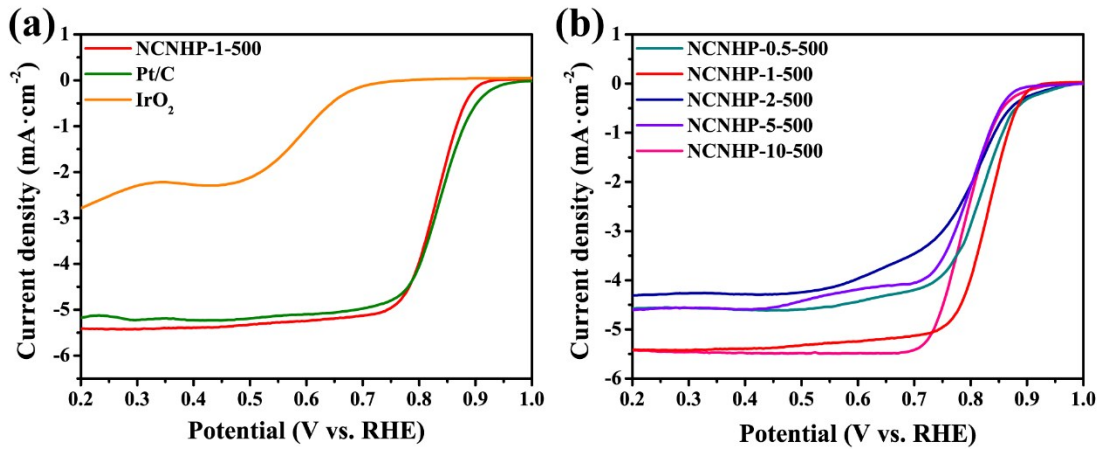

Figure S22. LSV curves of (a) NCNHP-1-500, commercial Pt/C and IrO_2, and (b) the NCNHP catalysts prepared by using different ZIF-67/KCl ratio in 0.1 M KOH for ORR.

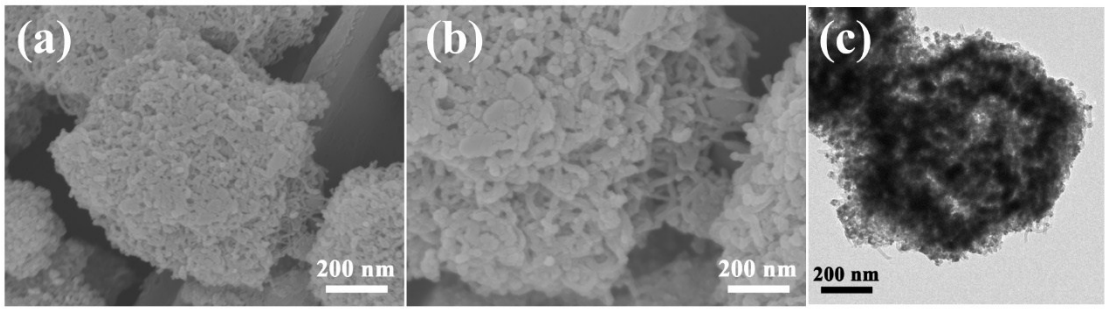

Figure S23. (a, b) SEM images and (c) TEM image of NCNHP-1-500 after stability test for ORR.

Table S1. BET surface areas and element contents of the catalysts.

Sample	BET surface area (m^2/g)	Element content [a] (wt%)		Relative content of the N species (%, based on XPS)			
		C	N	Graphitic N	Pyrrolic N	Pyridinic N	Co-N_x
NCNHP-1-400	157	43.21	1.17	15.04	36.84	39.76	8.36
NCNHP-1-500	152	37.81	3.27	16.67	25.72	35.14	22.46
NCNHP-1-600	147	40.69	1.90	24.51	25.49	33.82	16.18
NCNHP-1-700	146	40.58	1.34	29.10	24.74	32.97	13.19

(a) The weight percentage of C, N were determined by elemental analysis.

Table S2. The bifunctional activity of different catalysts for ORR and OER.

Catalyst	$E_{j=10}$ (V vs RHE)	$E_{1/2}$ (V vs RHE)	ΔE (V vs RHE)
NCNHP-1-400	1.584	0.801	0.783
NCNHP-1-500	1.540	0.828	0.712
NCNHP-1-600	1.566	0.814	0.752
NCNHP-1-700	1.574	0.807	0.767
Co/NPC-500	1.570	0.793	0.777
Pt/C	1.810	0.834	0.976
IrO_2	1.622	0.707	0.915
Pt/C+ IrO_2	-	-	0.788

Table S3. Summary of OER and ORR electrocatalytic activities of various Co-based electrocatalysts

Catalysts	**Loading ($mg \cdot cm^{-2}$)**	**OER performance**			**ORR performance**			**ΔE= $E_{j=10}$-$E_{1/2}$ (V vs RHE)**	**Ref.**
		Eletrolyte	Onset potential (V vs RHE)	$E_{j=10}$ (V vs RHE)	Eletrolyte	Onset potential (V vs RHE)	$E_{1/2}$ (V vs RHE)		
NCNHP-1-500	0.255	1M KOH	/	1.54	0.1M KOH	0.89	0.828	712	This work
Co-NC@Al_2O_3	0.28	1M KOH	/	1.647	0.1M KOH	0.91	0.86	787	S1
Co@NC-3/1	0.248	1M KOH	1.52	1.6	0.1M KOH	1.15	0.87	730	S2
Co_3O_4/HNCP-40	0.204	1M KOH	1.483	1.563	0.1M KOH	/	0.834	729	S3
Co_3O_4@C-MWCNTs	0.325	1M KOH	1.5	1.55	0.1M KOH	0.89	0.81	740	S4
Co_3ZnC/Co@CN	0.344	1M KOH	/	1.596	0.1M KOH	0.912	0.814	782	S5
Co@Co_3O_4@NC-900	2.5-3.0	1M KOH	/	1.6	0.1M KOH	/	0.8	800	S6
P-Co-NC-4	0.4	1M KOH	/	1.545	0.1M KOH	0.9	0.85	695	S7

Co@N-CNTF-2	0.28	1M KOH	/	1.58	0.1M KOH	0.91	0.81	770	S8
Co_4N/CNW/CC	0.2	1M KOH	/	1.54	0.1M KOH		0.8	740	S9
CoNi-MOF/rGO	0.6	1M KOH	/	1.548	0.1M KOH	0.88	0.718	830	S10
$Co_{0.85}Se$@NC	0.4	1M KOH	1.49	1.55	0.1M KOH	0.912	/	/	S11
D-Co@CNG	0.2	1M KOH	1.46	1.59	0.1M KOH	0.91	0.81	780	S12
CoO_x-NC	0.136	1M KOH	1.5	/	0.1M KOH	0.84	0.64	/	S13
Co_9S_8@TDC-900	1.4 OER 1.7 ORR	1M KOH	/	1.56	0.1M KOH	/	0.78	780	S14
$Co_{0.5}Fe_{0.5}S$@N-MC	0.8	1M KOH	1.57	1.64	0.1M KOH	0.913	0.808	832	S15
Co@Co_3O_4/NC-2	0.21	0.1M KOH	/	1.65	0.1M KOH	/	0.8	850	S16
Co_9S_8/C-NSs	0.25	0.1M KOH	1.5	1.664	0.1M KOH	0.892	0.778	886	S17
ZnCoNC-0.1	0.2	0.1M KOH	/	1.75	0.1M KOH	/	0.84	910	S18
CoZn-NC-700	0.24	0.1M KOH	/	1.62	0.1M KOH	0.98	0.84	780	S19
Co–N/PC@CNT-700	0.255	0.1M KOH	/	1.63	0.1M KOH	0.92	0.79	862	S20

References

(S1) Zhu, L.; Zheng, D.; Wang, Z.; Zheng, X.; Fang, P.; Zhu, J.; Yu, M.; Tong, Y.; Lu, X., A Confinement Strategy for Stabilizing ZIF-Derived Bifunctional Catalysts as a Benchmark Cathode of Flexible All-Solid-State Zinc-Air Batteries. *Adv. Mater.* **2018,** *30*, 1805268.

(S2) Li, Y.; Jia, B.; Fan, Y.; Zhu, K.; Li, G.; Su, C. Y., Bimetallic Zeolitic Imidazolite Framework Derived Carbon Nanotubes Embedded with Co Nanoparticles for Efficient Bifunctional Oxygen Electrocatalyst. *Adv. Energy Mater.* **2018,** *8*, 1702048.

(S3) Ding, D.; Shen, K.; Chen, X.; Chen, H.; Chen, J.; Fan, T.; Wu, R.; Li, Y., Multi-Level Architecture Optimization of MOF-Templated Co-Based Nanoparticles Embedded in Hollow N-Doped Carbon Polyhedra for Efficient OER and ORR. *ACS Catal.* **2018,** *8*, 7879-7888.

(S4) Li, X.; Fang, Y.; Lin, X.; Tian, M.; An, X.; Fu, Y.; Li, R.; Jin, J.; Ma, J., MOF

Derived Co_3O_4 Nanoparticles Embedded in N-doped Mesoporous Carbon Layer/MWCNT Hybrids: Extraordinary Bi-functional Electrocatalysts for OER and ORR. *J. Mater. Chem. A* **2015,** *3*, 17392-17402.

(S5) Su, J.; Xia, G.; Li, R.; Yang, Y.; Chen, J.; Shi, R.; Jiang, P.; Chen, Q., Co_3ZnC/Co Nano Heterojunctions Encapsulated in N-doped Graphene Layers Derived from PBAs as Highly Efficient Bi-functional OER and ORR Electrocatalysts. *J. Mater. Chem. A* **2016,** *4*, 9204-9212.

(S6) Guo, Z.; Wang, F.; Xia, Y.; Li, J.; Tamirat, A. G.; Liu, Y.; Wang, L.; Wang, Y.; Xia, Y., In Situ Encapsulation of Core-Shell-Structured Co@Co_3O_4 into Nitrogen-doped Carbon Polyhedra as a Bifunctional Catalyst for Rechargeable Zn-air Batteries. *J. Mater. Chem. A* **2018,** *6*, 1443-1453.

(S7) Liang, Z.; Zhang, C.; Yuan, H.; Zhang, W.; Zheng, H.; Cao, R., PVP-Assisted Transformation of a Metal-Organic Framework into Co-embedded N-enriched Meso/Microporous Carbon Materials as Bifunctional Electrocatalysts. *Chem. Commun.* **2018,** *54*, 7519-7522.

(S8) Guo, H.; Feng, Q.; Zhu, J.; Xu, J.; Li, Q.; Liu, S.; Xu, K.; Zhang, C.; Liu, T., Cobalt Nanoparticle-embedded Nitrogen-doped Carbon/Carbon Nanotube Frameworks derived from a Metal-Organic Framework for Tri-functional ORR, OER and HER Electrocatalysis. *J. Mater. Chem. A* **2019,** *7*, 3664-3672.

(S9) Meng, F.; Zhong, H.; Bao, D.; Yan, J.; Zhang, X., In Situ Coupling of Strung Co_4N and Intertwined N-C Fibers toward Free-Standing Bifunctional Cathode for Robust, Efficient, and Flexible Zn-Air Batteries. *J. Am. Chem. Soc.* **2016,** *138*, 10226-10231.

(S10) Zheng, X.; Cao, Y.; Liu, D.; Cai, M.; Ding, J.; Liu, X.; Wang, J.; Hu, W.; Zhong, C., Bimetallic Metal-Organic-Framework/Reduced Graphene Oxide Composites as Bifunctional Electrocatalysts for Rechargeable Zn-Air Batteries. *ACS Appl. Mater. Interf.* **2019,** *11*, 15662-15669.

(S11) Meng, T.; Qin, J.; Wang, S.; Zhao, D.; Mao, B.; Cao, M., In Situ Coupling of $Co_{0.85}Se$ and N-doped Carbon via One-step Selenization of Metal-Organic Frameworks as a Trifunctional Catalyst for Overall Water Splitting and Zn-Air

Batteries. *J. Mater. Chem. A* **2017,** *5*, 7001-7014.

(S12) Huang, Y.; Liu, Q.; Lv, J.; Babu, D. D.; Wang, W.; Wu, M.; Yuan, D.; Wang, Y., Co-Intercalation of Multiple Active Units into Graphene by Pyrolysis of Hydrogen-bonded Precursors for Zinc–Air Batteries and Water Splitting. *J. Mater. Chem. A* **2017,** *5*, 20882-20891.

(S13) Yiliguma, Y.; Wang, Z.; Xu, W.; Wang, Y.; Cui, X.; Al-Enizi, A. M.; Tang, Y.; Zheng, G., Bridged-Multi-Octahedral Cobalt Oxide Nanocrystals with a Co-terminated Surface as an Oxygen Evolution and Reduction Electrocatalyst. *J. Mater. Chem. A* **2017,** *5*, 7416-7422.

(S14) Zhao, J.; Wang, R.; Wang, S.; Lv, Y.; Xu, H.; Zang, S., Metal-Organic Framework-derived Co_9S_8 Embedded in N, O and S-tridoped Carbon Nanomaterials as an Efficient Oxygen Bifunctional Electrocatalyst. *J. Mater. Chem. A* **2019,** *7*, 7389-7395.

(S15) Shen, M.; Ruan, C.; Chen, Y.; Jiang, C.; Ai, K.; Lu, L., Covalent Entrapment of Cobalt-Iron Sulfides in N-doped Mesoporous Carbon: Extraordinary Bifunctional Electrocatalysts for Oxygen Reduction and Evolution Reactions. *ACS Appl. Mater. Interfaces* **2015,** *7*, 1207-1218.

(S16) Aijaz, A.; Masa, J.; Rosler, C.; Xia, W.; Weide, P.; Botz, A. J.; Fischer, R. A.; Schuhmann, W.; Muhler, M., $Co@Co_3O_4$ Encapsulated in Carbon Nanotube-Grafted Nitrogen-Doped Carbon Polyhedra as an Advanced Bifunctional Oxygen Electrode. *Angew. Chem. Int. Ed. Engl.* **2016,** *55*, 4087-4091.

(S17) Li, L.; Song, L.; Guo, H.; Xia, W.; Jiang, C.; Gao, B.; Wu, C.; Wang, T.; He, J., N-Doped Porous Carbon Nanosheets Decorated with Graphitized Carbon Layer Encapsulated Co_9S_8 Nnanoparticles: an Efficient Bifunctional Electrocatalyst for the OER and ORR. *Nanoscale* **2019,** *11*, 901-907.

(S18) Wu, X.; Meng, G.; Liu, W.; Li, T.; Yang, Q.; Sun, X.; Liu, J., Metal-Organic Framework-derived, Zn-doped Porous Carbon Polyhedra with Enhanced Activity as Bifunctional Catalysts for Rechargeable Zinc-Air Batteries. *Nano Res.* **2017,** *11*, 163-173.

(S19) Chen, B.; He, X.; Yin, F.; Wang, H.; Liu, D. J.; Shi, R.; Chen, J.; Yin, H.,

MO-Co@N-Doped Carbon (M = Zn or Co): Vital Roles of Inactive Zn and Highly Efficient Activity toward Oxygen Reduction/Evolution Reactions for Rechargeable Zn-Air Battery. *Adv. Funct. Mater.* **2017,** *27*, 1700795.

(S20) Ban, J.; Xu, G.; Zhang, L.; Xu, G.; Yang, L.; Sun, Z.; Jia, D., Efficient Co-N/PC@CNT Bifunctional Electrocatalytic Materials for Oxygen Reduction and Oxygen Evolution Reactions Based on Metal-Organic Frameworks. *Nanoscale* **2018,** *10*, 9077-9086.